EXPLORING EPITHELIAL-CELL CALCIUM SIGNALING WITH GEOMETRIC AND TOPOLOGICAL DATA ANALYSIS

Anonymous authors
Paper under double-blind review

ABSTRACT

Spatio-temporal calcium imaging is widely used to study neuronal activity. However the function of calcium signaling in epithelial cells is not well understood. We thus explore the underlying fluorescence patterns using a combination of data geometry and topology. We model the epithelial tissue as a graph and use a variant of geometric scattering transform (a multi-level wavelet transform on a graph) to describe the signaling at each time point. We then embed these discriptors using the manifold learning method PHATE in order to capture the entire time-trajectory of calcium signaling. Finally, we use persistent homology computed on the PHATE embedding to quantitatively characterize the trajectory. We demonstrate that scattering coefficients can effectively learn time point embeddings while PHATE can represent relationships between time points. Persistent homology provides a way to quantify differences between signaling dynamics as evidenced by the differences in dynamics between wild type cells and cells that are stalled in a particular cell cycle phase.

1 INTRODUCTION

Calcium ions play a significant role in transferring intercelluar signals and thus coordinating cellular behavior (Celli et al., 2011; Elias et al., 2002; Murata et al., 2018). Traditionally, calcium signaling has been studied via imaging techniques, particularly in neurons, where calcium signals act as charge carriers and intracellular messengers. However, calcium signaling is less well-studied in other tissues. Here we study patterns of time-varying calcium signaling in the basal stem cell layer of the skin epidermis where the function of the calcium signaling is not well known (Murata et al., 2018). Therefore, we pursue an unsupervised signaling pattern analysis here to try to derive hypotheses regarding signaling dynamics. In particular, we study the connection between cell cycle and calcium signaling by comparing the dynamics of wildtype cells with cells that are cycle-arrested.

We model the epithelial tissue as a nearest neighbors cellular graph $G = \{V, E\}$ with each vertex $v_i \in V$ being a cell, and $(v_j, v_k) \in E$ if the cells v_i and v_j are spatially adjacent. Since epithelial cells are arranged in planar spatial patterns, a graph where adjacent cells are those that touch at the cellular surfaces captures the tissue architecture. Then the calcium activity level of the cell is regarded as a *signal* x on the graph, i.e., each vertex v_i in the graph as activation value $x(v_i)$ representing the level of calcium activity. With this representation in place, we characterize the dynamics of calcium signaling first by deriving a descriptor of the spatial via geometric scattering transform (an extension of the original scattering transform on graphs) applied to the signal A (Gao et al., 2019).

After capturing the spatial pattern at each time point, we then represent the temporal variation of the spatial pattern using a non-linear dimensionality reduction method called PHATE (Moon et al., 2019). We choose PHATE because unlike many other dimensionality reduction methods, PHATE can preserve global multidimensional trajectory patterns in low dimensions without shattering their structure as tSNE/UMAP tend to do. The new PHATE coordinates can be used as a metric space in which to compute the more typical persistent homology based on Vietoris–Rips complexes (Rieck et al., 2020). This type of simplicial complex construction is based on increasing an ϵ threshold for connecting points based on distance, which in our case is the distance in the PHATE coordinate space.

We show that this method of analysis is useful for capturing the calcium signaling dynamics across a tissue, and allows us to visualize and quantitatively detect differences between complex signaling dynamics in the cellular state space.

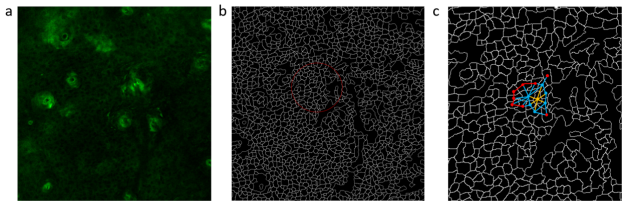

Figure 1: a. A snapshot of calcium fluorescence; b. cells from the snapshot with boundaries visualized; c. part of a cellular graph built for region highlighted in b.

2 METHOD

2.1 GEOMETRIC SCATTERING FOR TIME POINT EMBEDDING

A graph $G = (V, E)$ consisting of n vertices $V = \{v_1, \ldots, v_n\}$, and edges $E \subseteq \{(v_j, v_k) : 1 \leq j, k \leq n\}$ can be constructed for epidermal cells based on their spatial locations. We define the adjacency matrix of graph G as $\mathbf{A}$ and the corresponding degree matrix as $\mathbf{D}$. In this study we only considered unweighted graphs, which means $\mathbf{A}(v_j, v_k) = 1$ if $(v_j, v_k) \in E$ and 0 otherwise. $\mathbf{D}$ is given by $\mathbf{D}(v_j, v_j) = \sum_k \mathbf{A}(v_j, v_k)$, $\mathbf{D}(v_j, v_k) = 0$, $k \neq m$.

The raw signals $\mathbf{x}$ on the vertices are the fluorescence intensity for each cell at each time point. However, the relative signal intensity with respect to background signal (defined as the minimum fluorescence intensity for each cell during the 30 minutes experiment) better reflects the change of cell activities. Therefore, the raw signals were transformed as: $\mathbf{x} = (\mathbf{x} - \mathbf{x}_{min})/\mathbf{x}_{min}$ and normalized.

Our graph wavelets are designed based on lazy random walk $\mathbf{P} = \frac{1}{2}\left(\mathbf{I} + \mathbf{A}\mathbf{D}^{-1}\right)$ over graph:

$$\mathbf{\Psi}_0 = \mathbf{I} - \mathbf{P}\,, \quad \mathbf{\Psi}_j = \mathbf{P}^{2^{j-1}} - \mathbf{P}^{2^j} = \mathbf{P}^{2^{j-1}}(\mathbf{I} - \mathbf{P}^{2^{j-1}})\,, \quad j \geq 1\,. \tag{1}$$

The random walk $\mathbf{P}$ can be regarded as a low pass filter by retaining low frequency signals and suppressing high frequencies. We thus recover high frequencies information through performing multi-scale wavelet transform. The graph wavelet transform of signal $\mathbf{x}$ is constructed as $\mathbf{W}\mathbf{x} = \{\mathbf{P}^{2^J}\mathbf{x}\,,\, \mathbf{\Psi}_j\mathbf{x} : 1 \leq j \leq J\}$.

The spatial locations of cells remained unchanged during the experiments, but the signals kept changing along the time. We thus embedded each time point by calculating scattering coefficients for all the nodes at that time point. The zero order scattering coefficient were calculate as

$$S\mathbf{x} = \mathbf{P}^{2^J}\mathbf{x}(v_\ell) \tag{2}$$

As in Gao et al. (2019), the zero order scattering features can be augmented by first order scattering features via applying graph wavelets and extracting finer description of high frequency response of signal x. Specifically, the first order scattering coefficients for each time point were calculated as

$$S\mathbf{x}(j) = \mathbf{P}^{2^J}|\mathbf{\Psi}_j\mathbf{x}(v_\ell)|,\ 1 \leq j \leq J \tag{3}$$

and the second order scattering coefficients can be further obtained by

$$S\mathbf{x}(j, j', q) = \mathbf{P}^{2^J}|\mathbf{\Psi}_{j'}|\mathbf{\Psi}_j\mathbf{x}(v_\ell)||, 1 \leq j < j' \leq J \tag{4}$$

Finally, the zero order, first order and second order scattering coefficients were combined together as the embeddings for each time point.

2.2 PERSISTENT HOMOLOGY ANALYSIS OF PHATE TRAJECTORIES

The time point embeddings from geometric scattering form a matrix of $t \times m$, where t is the number of time points in the data and m is the number of scattering coefficients for each time point. We can visualize these embeddings by applying PHATE. We first calculated a distance matrix $\mathbf{D}$ based on Euclidean distance and applied an α-decaying kernel K to generate an affinity matrix as well as the diffusion operator $\mathbf{P}$. The optimal value t for diffusion is automatically chosen to be the knee point of the von Neumann entropy of $\mathbf{P}$. PHATE enables us to capture the variance from time point

embedding while still preserving the trajectory and global relations. The PHATE trajectory can thus reflect the time-varying patterns from calcium fluorescence data.

To have a quantitatively description of the generated PHATE trajectories, we calculated their persistent homology. The time point in the new PHATE coordinates form a point cloud X and we calculated the persistent homology based on the Vietoris-Rips filtration. Define the Vietoris-Rips complex of X as the filtered complex that contains a subset of X as a simplex if all pairwise distances in the subset are less than or equal to s, explicitly

$$VR_s(X) = \{[v_0, ...v_n] | \forall i, j \; d(i, j) \leq s\} \tag{5}$$

The Vietoris-Rips persistence of X is the persistent simplicial homology of $VR_s(X)$.

Finally we recorded the birth and death of topological features in the persistent diagram. In the diagram, each point indicates a topological feature in the trajectory which appears at a certain birth time and disappears at a death time. A point's distance from the diagonal therefore represents the persistence of the associated topological feature.

3 Applications and Results

3.1 Synthetic dataset

To validate the usefulness of our method, we first tested it on a synthetic dataset we created. We took a graph created from one of our calcium signalling samples with 1867 vertices (cells), and (1) we used a normalized graph Laplacian to diffuse a Dirac signal x centered on node i ($x_i = 1$) over the graph for 300 steps (illustrated in Appendix Fig. 7), which resulted in 300 signals, each more diffused than the previous. (2) Then we added normalized random noise $\epsilon \sim \mathcal{N}(\mu, \sigma^2)$ with $\mu = 0$ and $\sigma = 0.001$ to signals generated in (1). These perturbed signals are thus similar but not exactly the same to original ones. (3) For the Dirac signal x centered on node i, we further set $x_j = 1$ so that during diffusion initially it was similar to signals in (1) but would eventually diffuse to different patterns. We also diffused this signal for 300 steps. Finally we combined signals from (2) and signals from (1) to form a new 600-step signal, and signals from (3) were also combined with signals from (1) to form another series of signals of 600 steps. We calculated scattering coefficients for each time step and used PHATE to visualize them.

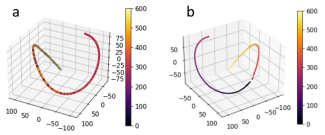

Figure 2: PHATE visualization of synthetic data for time points with a. similar but perturbed signals; b. totally different signals

As shown in Fig. 2a, time points with perturbed signals overlapped with time points with original signals, showing scattering transform and PHATE are invariant to small degrees of noise; while in Fig. 2b, time points from two signal sources formed two branches with their starting points near each other in PHATE coordinates. Thus from one end to the next this is akin to a signal condensing and then diffusing again. As expected, this creates a loop-like structure in the PHATE graph.

3.2 Calcium signaling experiment

We applied our method to data from optimized two-photon time-lapse imaging of live mice with a Ca^{2+}-sensor in all epidermal cells expressing Keratin 14 (K14-Cre; Rosa-CAG-LSL-GCaMP6s) (Chen et al., 2013; Mesa et al., 2018). To follow the cytosolic calcium dynamics in all basal epithelial cells, we took images every two seconds for a duration of 30 minutes across multiple adult mice. The spatial distribution with time-varying signals of cells form spatial-temporal patterns that may represent unique cell activities and interactions.

Spatial analysis of the signaling clusters during homeostasis revealed non radial patterns when initiating cells propagated signal to their neighbors (as shown in Appendix Fig.4). These results seem to suggest that neighboring cells might have different competencies to participate in Ca^{2+} signaling. Given basal cells asynchronously transition through the cell cycle phases, we hypothesized that clusters of cells may have different abilities to propagate calcium depending on what phase of the cell cycle individual cells may be at. To test this hypothesis, we genetically stall cells at $G1$ stage to see if calcium signaling patterns are changed. Under this system we wish to mathematically characterize the spatial-temporal patterns before and after interventions. We tested our proposed method on this calcium signalling dataset which contains both wide type cells and cells that are stalled at $G1$ stage. These two types of cells generate different spatio-temporal fluorescence patterns

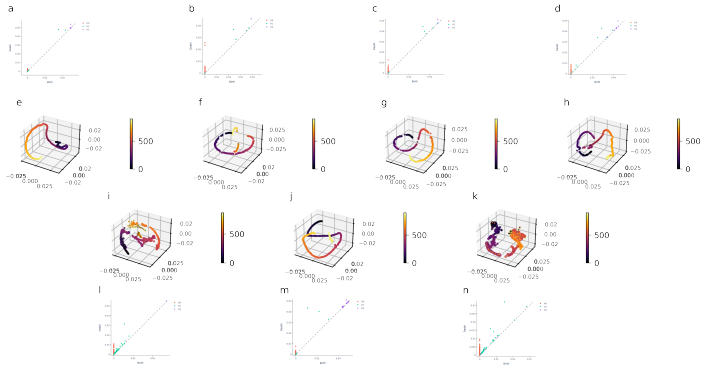

Figure 3: PHATE visualization of time point embeddings from control group (e, f, g, and h) and positive group (i, j, and k). The corresponding persistence diagram was shown on the top for control group (a, b, c, and d) and at the bottom for positive group (l, m, and n)

we tried to retrieve. We first showed that the geometric scattering transform for time point embedding captures the fluorescence variability via the visualization through PHATE, then we compared the differences of PHATE trajectories utilizing persistent homology in Fig. 3.

3.3 Comparison of PHATE trajectories on two types of cells

Wild type cells were used as control group to cells that were stalled at $G1$ stage which we referred as *positive* group below. There were a total of four duplicates from control group and three duplicates from positive group, from which we built four and three graphs respectively. We generated scattering coefficients for each time point from each graph. Then we applied PHATE and visualized the embeddings. Each time point was colored based on the corresponding time point id. In Fig. 3, we compared PHATE trajectories for time points from control group and positive group. The time point embeddings from control group (Fig. 3e, 3f, 3g, and 3h) formed smooth trajectories along time, suggesting the change of signals over graph were generally steady. This also matched with our observation that there were fewer single cell flashing or small waves of flashes in control group. In contrast, PHATE for positive group in Fig. 3i, 3j, and 3k showed different and more complex patterns with loops or holes in the trajectories. This may be caused by rapid change of signals over the graph: more single cell flashes and shorter lingering time may contribute to this.

3.4 Topological feature analysis

We performed topological data analysis using persistent homology to quantatively (rather than qualitatively) compare PHATE trajectories. The persistence diagram from control group (Fig. 3a, 3b, 3c, and 3d) and positive group (Fig. 3l, 3m, and 3n) were compared. $H0$ features represent connected components in the trajectory, $H1$ features represent loops and $H2$ represent voids. There were fewer $H1$ features from the persistent diagrams for control group, and many of them were created and died at a later stage. The persistence of $H1$ features were also in general shorter than those in positive group. On the other hand, in positive groups most $H1$ features usually appeared and disappeared at earlier stage. As a comparison, we also included results from activation filtration in Appendix. A.6, which showed a similar pattern for positive and control groups but with much more noisy illustration. These differences from persistence diagram suggest different topological features for PHATE trajectories and hence different calcium fluorescence patterns in these two types of cells.

4 Conclusion

We present an unsupervised approach for uncovering calcium signalling patterns from epithelial cells. Our approach combines data geometry, graph signal processing as well as topology to represent signals and their time-varying dynamics. These representations allowed us to explore the signaling dynamics in the novel context of epithelial cells, where regular dynamics are smoother and undergo larger loops than cell-cycle halted dynamics. This suggests that cell cycle is related to signaling competency of cells. Future work will involve associating topological features with signaling features.

REFERENCES

A Celli, DS Mackenzie, DS Crumrine, CL Tu, M Hupe, DD Bikle, PM Elias, and TM Mauro. Endoplasmic reticulum ca2+ depletion activates xbp1 and controls terminal differentiation in keratinocytes and epidermis. *British Journal of Dermatology*, 164(1):16–25, 2011.

Baohui Chen, Luke A. Gilbert, Beth A. Cimini, Joerg Schnitzbauer, Wei Zhang, Gene-Wei Li, Jason Park, Elizabeth H. Blackburn, Jonathan S. Weissman, Lei S. Qi, and Bo Huang. Dynamic imaging of genomic loci in living human cells by an optimized crispr/cas system. *Cell*, 155(7): 1479–1491, 2013. ISSN 0092-8674. doi: https://doi.org/10.1016/j.cell.2013.12.001. URL https://www.sciencedirect.com/science/article/pii/S0092867413015316.

Ronald R. Coifman and Mauro Maggioni. Diffusion wavelets. *Applied and Computational Harmonic Analysis*, 21(1):53–94, 2006.

Peter M Elias, Barbara E Brown, Debra Crumrine, Kenneth R Feingold, and Sung K Ahn. Origin of the epidermal calcium gradient: regulation by barrier status and role of active vs passive mechanisms. *Journal of investigative dermatology*, 119(6):1269–1274, 2002.

Fernando Gama, Alejandro Ribeiro, and Joan Bruna. Diffusion scattering transforms on graphs. In *International Conference on Learning Representations*, 2019.

Feng Gao, Guy Wolf, and Matthew Hirn. Geometric scattering for graph data analysis. In Kamalika Chaudhuri and Ruslan Salakhutdinov (eds.), *Proceedings of the 36th International Conference on Machine Learning*, volume 97 of *Proceedings of Machine Learning Research*, pp. 2122–2131. PMLR, 09–15 Jun 2019. URL http://proceedings.mlr.press/v97/gao19e.html.

Kailin R. Mesa, Kyogo Kawaguchi, Katie Cockburn, David Gonzalez, Jonathan Boucher, Tianchi Xin, Allon M. Klein, and Valentina Greco. Homeostatic epidermal stem cell self-renewal is driven by local differentiation. *Cell Stem Cell*, 23(5):677–686.e4, 2018. ISSN 1934-5909. doi: https://doi.org/10.1016/j.stem.2018.09.005. URL https://www.sciencedirect.com/science/article/pii/S1934590918304429.

Kevin R. Moon, David van Dijk, Zheng Wang, Scott Gigante, Daniel B. Burkhardt, William S. Chen, Kristina Yim, Antonia van den Elzen, Matthew J. Hirn, Ronald R. Coifman, Natalia B. Ivanova, Guy Wolf, and Smita Krishnaswamy. Visualizing structure and transitions in high-dimensional biological data. *Nature Biotechnology*, 37(12):1482–1492, December 2019.

Teruasa Murata, Tetsuya Honda, Gyohei Egawa, Yasuo Yamamoto, Ryo Ichijo, Fumiko Toyoshima, Teruki Dainichi, and Kenji Kabashima. Transient elevation of cytoplasmic calcium ion concentration at a single cell level precedes morphological changes of epidermal keratinocytes during cornification. *Scientific reports*, 8(1):1–10, 2018.

Bastian Rieck, Tristan Yates, Christian Bock, Karsten Borgwardt, Guy Wolf, Nick Turk-Browne, and Smita Krishnaswamy. Uncovering the topology of time-varying fMRI data using cubical persistence. In *Advances in Neural Information Processing Systems 33 (NeurIPS)*. Curran Associates, Inc., 2020.

A APPENDIX

A.1 DIFFUSION GEOMETRY

To better capture local affinities for all pairs of points in a dataset, one of the common approaches is to construct a distance matrix using a predefined distance function and apply kernel functions to transform these global distances to local similarities. As showed in Coifman & Maggioni (2006), a graph can be built from discrete data with affinities

$$(\boldsymbol{W}_\epsilon)_{ij} := e^{-\|x_i - x_j\|_2^2/\epsilon} \tag{6}$$

However, the direct embedding of local affinities can result in a loss of global structures. Therefore a Markov diffusion operator $\boldsymbol{T}$ defined on the dataset can be used to travel along the intrinsic geometry structure of the data manifold and preserve the overall structure of data. This diffusion operator $\boldsymbol{T}$ can be defined as

$$\boldsymbol{T}_\epsilon := \boldsymbol{D}^{-1}\boldsymbol{M}_\epsilon, \text{ where } \boldsymbol{M}_\epsilon := \boldsymbol{Q}^{-1}\boldsymbol{K}_\epsilon\boldsymbol{Q}^{-1}. \tag{7}$$

Both $\boldsymbol{D}$ and $\boldsymbol{Q}$ are diagonal matrices calculated as $\boldsymbol{D}_{ii} := \sum_j (\boldsymbol{M}_\epsilon)_{ij}$ and $\boldsymbol{Q}_{ii} := \sum_j (\boldsymbol{K}_\epsilon)_{ij}$. By calculating the tth power of the diffusion operator, we can capture multiscale local neighborhoods of data points up to scale t, where locality is considered via random walks that propagate over the intrinsic manifold geometry of the data.

A.2 GEOMETRIC SCATTERING

Geometric scattering transform is an unsupervised method for generating embeddings for graph-structured data (Gao et al., 2019). It is constructed by applying a cascade of graph wavelet transform followed by nonlinear modulus operation such as absolute value nonlinearity (Gao et al., 2019; Gama et al., 2019). Graph wavelets are designed based on lazy random walks $\mathbf{P} = \frac{1}{2}\left(\mathbf{I} + \mathbf{A}\mathbf{D}^{-1}\right)$ over graph:

$$\boldsymbol{\Psi}_0 = \mathbf{I} - \mathbf{P}\,, \quad \boldsymbol{\Psi}_j = \mathbf{P}^{2^{j-1}} - \mathbf{P}^{2^j} = \mathbf{P}^{2^{j-1}}(\mathbf{I} - \mathbf{P}^{2^{j-1}})\,, \quad j \geq 1\,. \tag{8}$$

The multi-scale nature of graph wavelets allows geometric scattering transform to traverse the entire graph in one layer, which provides both local and global graph features. Summation of the signal responses is used to to obtain invariant graph-level features. Finally, the zero-order scattering coefficients are calculated by taking statistical moments of the summation of signals, and the first order features are obtained by applying graph wavelet which aggregates multiscale information of the graph. Second order geometric scattering features can further augment first order features by iterating the graph wavelet and absolute value transforms. The collection of graph scattering features provides a rich set of multiscale invariants of the graph G and can be used under both supervised and unsupervised settings for graph embedding.

A.3 PHATE

PHATE is a dimensionality-reduction method that captures both local and global nonlinear structure through constructing a diffusion geometry (Moon et al., 2019). It computes local similarities between data points, and diffuses through the data using a Markovian random-walk diffusion process to infer global relations andrepresent shape of the data.

Given a $n \times m$ data matrix $\mathbf{N}$, where n is the number of data points and m the number of features, PHATE first computes the pairwise distance matrix $\mathbf{M}$ using a predefined distance function ϕ with $\mathbf{M}_{ij} = \phi(\mathbf{N}_{i,:}, \mathbf{N}_{j,:})$. As we described in Sec. A.1, an affinity matrix $\mathbf{W}$ is computed to reflect local similarities. Specifically, PHATE utilizes an α-decaying kernel with a locally-adaptive bandwidth $\epsilon_{k,i}$ corresponding to the k-NN distance of the i-th data point. The elements of $\mathbf{W}$ are given by:

$$\mathbf{W}_{i,j} = K_{k,\alpha}(i,j) = \frac{1}{2}\exp\left(-\left(\frac{\boldsymbol{M}_{i,j}}{\epsilon_{k,i}}\right)^\alpha\right) + \frac{1}{2}\exp\left(-\left(\frac{\boldsymbol{M}_{i,j}}{\epsilon_{k,j}}\right)^\alpha\right)$$

The decaying factor α regulates the decay rate of the kernel (smaller $\alpha \Rightarrow$ kernel with lighter tails), $\alpha = 2$ corresponding to the Gaussian.

The diffusion operator $\mathbf{T}$ can then be obtained by calculating the row-sum of the affinity matrix with element $\mathbf{T}_{i,j}$ giving the probability of moving from the i-th to the j-th data point in one time

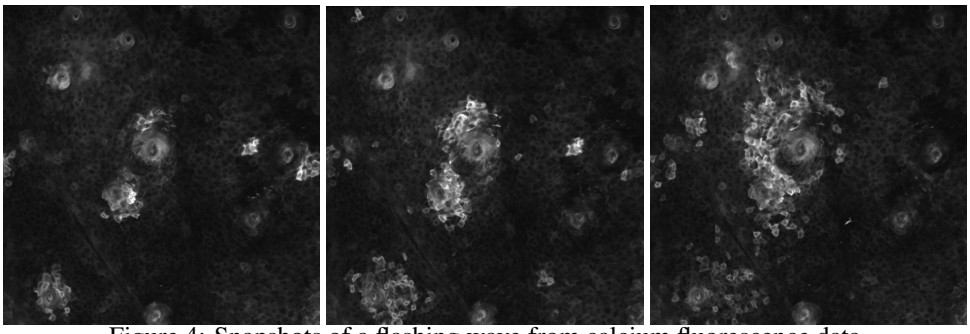

Figure 4: Snapshots of a flashing wave from calcium fluorescence data

step. The global structure of the data can be further learned through calculating the tth power of the diffusion operator $\mathbf{T}$, which propagates affinity of the data through diffusion up to a scale of t.

Finally, PHATE conducts dimensionality reduction while retaining diffusion geometry information obtained from $\mathbf{T}$ by defining a pairwise *potential distance* as $\mathbf{ID}_{i,j} = \| \log \boldsymbol{T}_{i,:} - \log \boldsymbol{T}_{j,:} \|_2$ between corresponding t-step diffusion probability distributions of the two points. This preserves the *global context* for each data point. The resulting information distance matrix $\mathbf{ID}$ is finally embedded into a low dimensional (2D or 3D) space by metric multidimensional scaling (MDS), and makes it possible to visualize intrinsic geometric information from data.

A.4 Persistent homology

Simplicial homology calculates a sequence of homology groups for describing the topological features of a simplicial complex K and measuring its connectivity. Persistent homology is an extension of simplicial homology that requires a simplicial complex K and an additional function $f\colon \mathrm{K} \to \mathbb{R}$. If f only attains a finite set of function values $f_0 \leq f_1 \leq \cdots \leq \ldots f_{m-1} \leq f_m$, then K can be sorted according to these values, leading to a *filtration* of K, i.e., a nested sequence of simplicial complexes $\emptyset = \mathrm{K}_0 \subseteq \mathrm{K}_1 \subseteq \cdots \subseteq \mathrm{K}_{m-1} \subseteq \mathrm{K}_m = \mathrm{K}$, with $\mathrm{K}_i := \{\sigma \in K \mid f(\sigma) \leq f_i\}$. Filtrations model the evolution of K along f and permit tracking whether topological features are *created* or *destroyed*. Persistent homology represents each topological feature as a tuple $(f_i, f_j) \in \mathbb{R}^2$, with $i \leq j$ and $f_i, f_j \in \mathrm{im}(f)$. These tuples are collected in a *persistence diagram* $\mathcal{D}_d$, which contains the birth and death times of the features as a point, thus summarizing all d-dimensional topological features.

A.5 Snapshots of flashing waves

Snapshots of a large flashing wave was shown in Fig. 4. The signaling cluster revealed non-radial patterns when initiating cells propagated signal to their neighbors.

A.6 Activation filtration

As an comparison to PHATE visualization of scattering coefficients, we also calculated persistent diagram using activation filtration for both control and positive groups. The $D0$ and $D1$ features were shown in Fig. 5 and Fig. 6 respectively. They were arranged in the same order as in Fig. 3. The birth time of $D0$ features from positive groups were in general smaller than those in the control group, especially for samples demonstrated in Fig. 5e and Fig. 5g. In addition, the death time of $D1$ features from Fig. 6 for positive groups were smaller than control group.

A.7 Diffusion of a Dirac signal on graph

Here we show an example of how a Dirac signal defined on one of the cells is diffused by a normalized graph Laplacian in Fig. 7. The signal starts from one cell, then diffuses to its surrounding cells in a few steps.

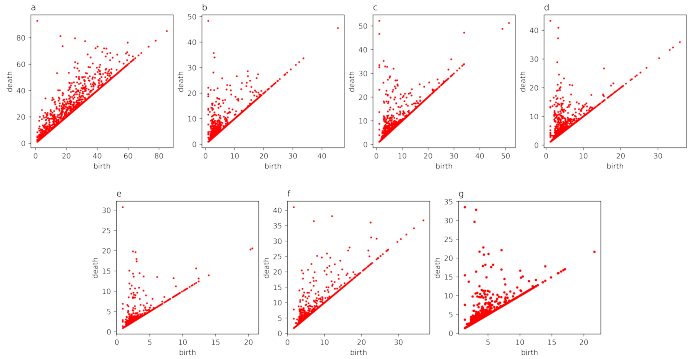

Figure 5: Persistent diagram of $D0$ feature from activation filtration for control group (a, b, c, and d) and positive group (e, f, and g)

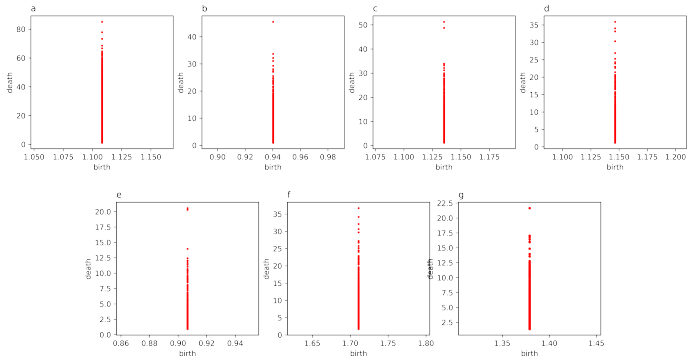

Figure 6: Persistent diagram of $D1$ feature from activation filtration for control group (a, b, c, and d) and positive group (e, f, and g)

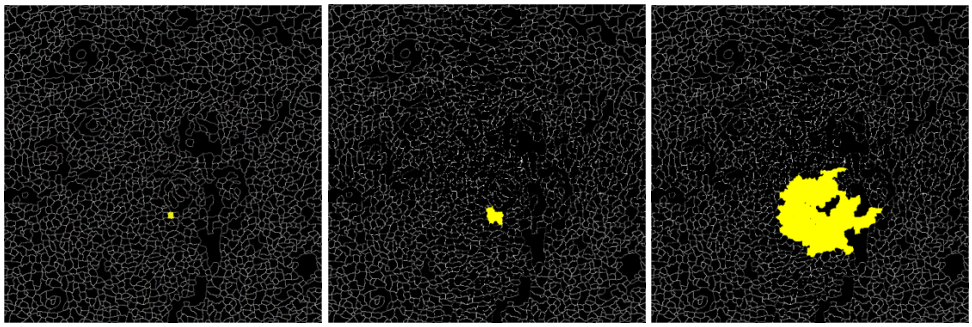

Figure 7: Diffusion of a Dirac signal on graph at time step 0, 1 and 5 from left to right